https://doi.org/10.2352/CIC.2023.31.1.13

Optimised Spherical Sampling of the Object Colour Solid

H.J. Rivertz [1], *M. Mackiewicz* [2]; [1] *Norwegian University of Science and Technology, Trondheim, Norway;* [2] *University of East Anglia, Norwich, UK*

Abstract

We propose a new method for approximating object colour solids, which we call Optimised Spherical Sampling. We compare our new method to the previously described methods based on 1) the two-transition conjecture of Schrodinger and 2) Random Spherical Sampling. The proposed method is based on the approximation of the OCS local error at every face of the volume and its subsequent optimisation. We find that the new method produces a significantly less error for the same number of samples than the two prior art methods.

1 Introduction

Objects reflecting light exhibit a range of colors, which are encompassed within a closed convex 3-D volume known as the object color solid (OCS). In Figure 1, we present the OCS generated for illuminant A in the CIE 1931 color space (XYZ) [3]. Points located within the interior of the object-color solid represent distinct metameric classes, wherein each class corresponds to an infinite number of reflectance spectra. Conversely, each point on the surface of the object-color solid corresponds to a unique reflectance spectrum. These surface spectra, referred to as optimal, are given by elementary step functions with transitions at given wavelengths $\lambda_1, \lambda_2, \cdots, \lambda_m$ if and only if the above set of transition wavelengths are the only zero-crossings of the equation $\mathbf{k} \cdot \mathbf{s}(\lambda)$, where $\mathbf{k}$ is a real non-zero vector and $\mathbf{s}(\lambda)$ is the product $e(\lambda)\mathbf{c}(\lambda)$ of an illuminant spectrum and the set of spectral sensitivity functions $\mathbf{c}(\lambda)$ [4, 5, 6, 7].

For a nonzero illumination function, the optimal spectrum is given by

$$\rho_{\mathbf{k}}(\lambda) = \begin{cases} 0, & \mathbf{k} \cdot \mathbf{c}(\lambda) < 0 \\ 1, & \mathbf{k} \cdot \mathbf{c}(\lambda) \geq 0 \end{cases}. \tag{1}$$

Fig. 2 shows how an optimal spectrum is created using Eq. 1. The corresponding tri-stimuli is calculated by the formula

$$\Phi(\rho_{\mathbf{k}}) = \int_{\lambda_{min}}^{\lambda_{max}} \rho_{\mathbf{k}}(\lambda)\mathbf{s}(\lambda)\mathrm{d}\lambda. \tag{2}$$

This gives a map from the unit sphere to the OCS. This map is known as the inverse of the Gauss map from differential geometry. The Gauss map sends each point on the surface to the outward pointing unit normal vector. Figure 1 shows an OCS. The sharp edges marked with red and blue colour are called meridians. A point on a meridian is the image of many vectors $\mathbf{k}$.

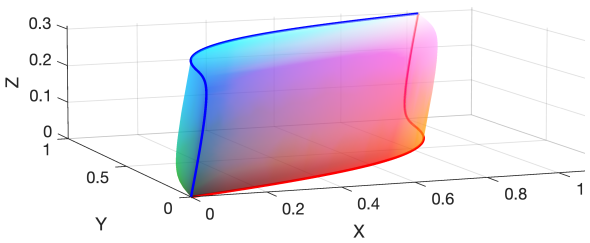

Figure 1: The OCS comprises two sheets glued along the meridians (curves marked with red and blue colour). The optimal spectra corresponding to the points on these two curves have only one transition wavelength. The blue line represents optimal object colours that reflects light with wavelength shorter than the transition wavelength.

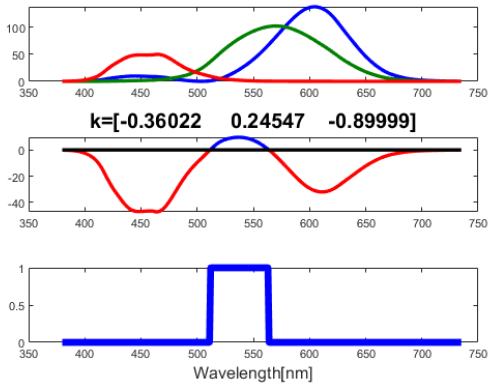

Figure 2: An illustration how to find an optimal spectrum for a given vector $\mathbf{k}$. XYZ colour matching functions multiplied by the D65 illuminant (top). The linear combination (with $\mathbf{k}$ coefficients) of the above three functions (middle). Corresponding optimal spectrum (bottom).

A finite set of normal vectors gives a sampling set Ω of optimal tri-stimuli. The convex hull of this set gives a lower bound approximation L_Ω of the OCS.

The vector $\mathbf{k}$ is a normal vector on the boundary of the OCS. In fact, the OCS is the intersection of all half spaces defined by

$$H_{\mathbf{k}} = \left\{ \mathbf{x} \,\middle|\, \mathbf{k} \cdot \left(\mathbf{x} - \Phi(\rho_{\text{opt}}) \right) \leq 0 \right\}. \tag{3}$$

Restricted to the subset of the OCS normal vectors, the above intersection gives an upper bound approximation U_Ω of the OCS. We have

$$L_\Omega \subset OCS \subset U_\Omega. \tag{4}$$

In this paper, we will compare the accuracy of lower bound approximations obtained using three methods. The first method uses Schrodinger's conjecture on optimal spectra [1, 8]. It states that optimal spectra have at most two transitions. This conjecture is mostly true, with some exceptions[2]. In the second method, we generate the optimal spectra from a set of random normal vectors [5, 6].

The third method is the new method which is proposed in this paper. As in the second method, we generate the optimal spectra from a set of normal vectors. However, in contrast to the second method, we propose to use a local error measure and an optimisation algorithm.

The rest of the paper is organised as follows. In Section 2, we describe the local error measure of the the object colour solid approximations. In Section 3, we propose an algorithm which utilises spherical sampling informed by the minimisation of the

said error measure to construct object colour solids with a reduced error or fewer points than the prior art. In Section 4, we evaluate our method in comparison to the aforementioned prior art methods. We conclude and discuss pottential future work in Section 5

2 On the local error

The difference between L_Ω and U_Ω has the following local description. The surface of L_Ω consists of triangles. Consider a triangle with vertices $\mathbf{q}_1, \mathbf{q}_2, \mathbf{q}_3 \in \mathbb{R}^3$. Each vertex $\mathbf{q}_k$ has an associated normal vector $\mathbf{n}_k$. This is through the spherical parametrisation of the surface. Each normal vector $\mathbf{n}_k$ defines a tangent plane $T_{\mathbf{q}_k}$ at $\mathbf{q}_k$ defined by $\mathbf{n}_k \cdot (\mathbf{x} - \mathbf{q}_k) = 0$. These tangent planes intersect in a point $c \in U_\Omega$ that lies outside the OCS at a vertex of U_Ω. Let $\mathbf{a} = [\mathbf{n}_1 \cdot \mathbf{q}_1, \mathbf{n}_2 \cdot \mathbf{q}_2, \mathbf{n}_3 \cdot \mathbf{q}_3]^T$. We find point $\mathbf{v}$ at the intersection of the said tangent planes by solving the system $N^T \mathbf{x} = \mathbf{a}$, where N is the 3×3 matrix with the $\mathbf{n}_k$ vectors in its columns. The solution is $\mathbf{v} = (N^T)^{-1}\mathbf{a}$.

The triangular faces of the solid are glued together along their edges. Figure 3 shows a typical local error solid. In order to build this solid, we consider the intersection L_k between two tangent planes as shown in the figure. That is the line through $\mathbf{v}$ and $\mathbf{p}_k$.

Let E_1 be the edge connecting $\mathbf{q}_2$ and $\mathbf{q}_3$ and let L_1 be the intersection between the tangent planes $T_{\mathbf{q}_2}$ and $T_{\mathbf{q}_3}$. The point $\mathbf{p}_1$ is the point on L_1 with shortest distance to E_1.

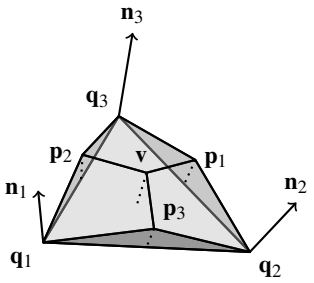

Figure 3: The local error solid over the triangle with vertices $\{\mathbf{q}_1, \mathbf{q}_2, \mathbf{q}_3\}$. There are 4 additional points, the point $\mathbf{v}$ is the intersection of the tangent planes at these vertices. The tangent planes at $\mathbf{q}_1$ and $\mathbf{q}_2$ intersect in a line. $\mathbf{p}_3$ is the point on this line closest to the edge between $\mathbf{q}_1$ and $\mathbf{q}_2$. The points $\mathbf{p}_1$ and $\mathbf{p}_2$ are defined analogously.

This is found by using the Lagrangian multiplier method for minimizing $\|\mathbf{x} - t_2\mathbf{q}_2 - t_3\mathbf{q}_3\|^2$ under the constraints

$$t_2 + t_3 = 1, \tag{5}$$

$$\mathbf{n}_2 \cdot (\mathbf{x} - \mathbf{q}_2) = 0, \quad \text{and} \tag{6}$$

$$\mathbf{n}_3 \cdot (\mathbf{x} - \mathbf{q}_3) = 0. \tag{7}$$

The points $\mathbf{p}_2$ and $\mathbf{p}_3$ are constructed analogously. For each of the points $\mathbf{p}_1$, $\mathbf{p}_2$, and $\mathbf{p}_3$, we find distance to the corresponding edge. We also compute the distance between $\mathbf{v}$ and the $\mathbf{q}_1\mathbf{q}_2\mathbf{q}_3$-triangle. The largest of these four distances is our measure of error used in the next section. Since two sampling vectors can give the same tri-stimulus, we also consider the local error solids over degenerate triangles as shown in Figure 4.

3 Constructing the object colour solid

In this section we describe the proposed Optimised Spherical Sampling algorithm for the construction of object colour solids. The algorithm is given in Algorithm 1. The subsequent subsections describe consecutive steps of the algorithm.

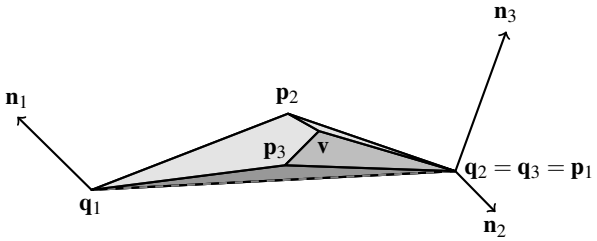

Figure 4: The local error solid over a degenerate triangle with vertices $\{\mathbf{q}_1, \mathbf{q}_2 = \mathbf{q}_3\}$. There are 3 additional points, the point $\mathbf{v}$ is the intersection of the tangent planes at these vertices. The tangent planes at $\mathbf{q}_1$ and the tangent plane $\mathbf{q}_2$ corresponding to the normal vector $\mathbf{n}_2$ intersect in a line. $\mathbf{p}_3$ is the point on this line closest to the edge between $\mathbf{q}_1$ and $\mathbf{q}_2$. The point $\mathbf{p}_3$ is defined analogously.

Algorithm 1 Creating optimised OCS

1. Choose 10 initial normal vector samples as described in Section 3.1
2. The newly added vectors are adjusted as explained in Section 3.2.
3. A triangulation of the vectors is computed by using a regularised OCS. This is described in Section 3.3. The sole purpose of the regularised OCS is to produce the triangulation.
4. For each triangle in the vector triangulation, we approximate a local upper bound of the error for the triangle. The error is defined in Section 2.
5. For each triangle $\mathbf{n}_1\mathbf{n}_2\mathbf{n}_3$ with error greater than the tolerance tol produce a new vector sample equal to $(\mathbf{n}_1 + \mathbf{n}_2 + \mathbf{n}_3)/\|\mathbf{n}_1 + \mathbf{n}_2 + \mathbf{n}_3\|$.
6. All vector samples that are surrounded by triangles with local error less than $tol/10$ are removed from the sampling vector set.
7. The algorithm stops if the number of vector samples stops increasing or after a given number of iterations.
8. Go to step 2.

3.1 The initial approximation

We start by choosing two sets of unit vectors. First, from the standard basis we obtain a set of six vectors $\{\pm\mathbf{e}_1, \pm\mathbf{e}_2, \pm\mathbf{e}_3\}$. These vectors correspond to black and white points. To construct the convex hull, we need more points. We choose the following two pairs of vectors: $\{(\mathbf{e}_1 - \mathbf{e}_2)/\sqrt{2}, (\mathbf{e}_2 - \mathbf{e}_1)/\sqrt{2}\}, \{(\mathbf{e}_3 - \mathbf{e}_2)/\sqrt{2}, (\mathbf{e}_2 - \mathbf{e}_3)/\sqrt{2}\}\}$. The first pair of vectors gives two transitions. These are located at $\lambda_1 = 473.5$nm and $\lambda_2 = 577.5$nm.

The initial approximation of the OCS is displayed in Figure 5. The optimal spectrum with the two transitions above corresponds to the magenta/green vertex. The second pair of vectors gives a one transition optimal spectrum located at the wavelength $\lambda_1 =$ 495.5nm, which corresponds to the blue/yellow vertex.

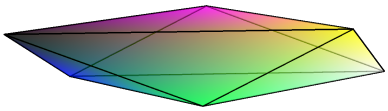

Figure 5: The first approximation of the OCS is a skew octahedron. The colours in this and subsequent figures are for illustration only. We converted from XYZ to sRGB followed by a linear white balance and clipping of the values to the unit interval.

3.2 Adjusting normal vectors for less than 2 transition spectra

For one-transition optimal spectra, there are infinite number of vectors $\mathbf{k}$ giving the same transition wavelength λ. Let λ be between two sampling wavelengths for the colour matching function. Let $\lambda^{\pm} = \lambda \pm \Delta\lambda/2$, where $\Delta\lambda$ is the sampling interval for $\mathbf{c}$. The set of candidates for $\mathbf{k}$ is obtained from the equation $\mathbf{k} \cdot \left(\mathbf{c}(\lambda^-) + \mathbf{c}(\lambda^+)\right)$.

To be efficient in our choice of $\mathbf{k}$, we choose such $\mathbf{k}$ vectors which are close to vectors that produce two transitions or more. In other words, we choose a vector that is close to a normal vector on one of the two sheets of the OCS. We achieve this by considering a $\mathbf{k}$ vector that gives transitions at either end of the visible spectrum denoted as $\lambda_{\max}$ and $\lambda_{\min}$. We use Algorithm 2 to adjust $\mathbf{k}$. We obtain two new vectors. First we use the algorithm with $\lambda_0 = \lambda_{max}$ and then we use the algorithm $\lambda_0 = \lambda_{min}$.

Figures 6 and 7 show the effect of adjusting the normal vectors for less than two transition spectra in contrast to randomly selected normal vectors.

Algorithm 2 Vector adjustment.

In case of one transition optimal spectrum, there are two equations

$$\begin{aligned} \mathbf{k} \cdot \left(\mathbf{c}(\lambda^-) + \mathbf{c}(\lambda^+)\right) &= 0 \text{ and} \\ \mathbf{k} \cdot \mathbf{c}(\lambda_0) &= 0. \end{aligned}$$

The solution of this system is a line V. In case of no transitions, we have one equation $\mathbf{k} \cdot \mathbf{c}(\lambda_0) = 0$. The solution of this equation is a plane V. We now use the following algorithm.

procedure
  $\mathbf{k}' \leftarrow$ projection of $\mathbf{k}$ onto V
  $\mathbf{k}' \leftarrow \mathbf{k}'/\|\mathbf{k}'\|$
  if $\mathbf{k}'$ gives exactly one transition **then return** $\mathbf{k}'$
loop:
  $\mathbf{k}'' = (\mathbf{k} + \mathbf{k}')/\|\mathbf{k} + \mathbf{k}'\|$
  if $\mathbf{k}''$ gives exactly one transition **then**
    $\mathbf{k} \leftarrow \mathbf{k}''$
  else
    $\mathbf{k}' \leftarrow \mathbf{k}''$
  if $\mathbf{k}' = \mathbf{k}$ **then return** $\mathbf{k}$
  if Max iterations **then return** $\mathbf{k}$

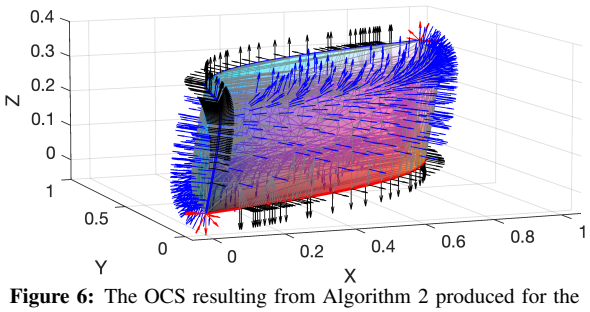

Figure 6: The OCS resulting from Algorithm 2 produced for the CIE 1931 CMFs and the illuminant A. The red vectors correspond to zero transition spectra i.e. the black or the white points. The black vectors correspond to the one-transition spectra on the meridians and the blue vectors corresponds to optimal spectra with more than 1 transition.

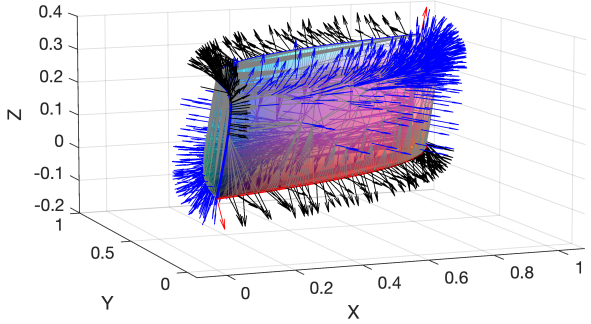

Figure 7: As in Figure 6, but for the random spherical sampling.

3.3 The regularised OCS

The adjustments of the vectors in the previous section result in two or more vectors representing the same tri-stimulus. However, these two vectors are far from each other on the unit sphere. This is shown in Figure 6. Note, the angle between some of the vectors on the two meridians is approximately 90 degrees, but they correspond to the same one-transition optimal spectrum and therefore the same point on the OCS. In order to make a triangulation of the OCS that has similar object colours on the edges of each face (triangle), we use the idea of surface regularisation.

For each vector $\mathbf{k}$, we calculate the point given by $\Phi(\rho_{\mathbf{k}}) + \varepsilon\mathbf{k}$. The new surface is the regularised OCS. We used $\varepsilon = 0.1$ in our calculations. We calculate the convex hull of the regularised OCS approximation R_Ω. Figure 8 and Figure 9 show regularised OCSs with varying numbers of faces.

4 Experiments and Results

We conducted our experiments with two different sets of colour matching functions (CIE 1931 2°, XYZ CMFs [3, 9] and the more recent CIE physiologically-relevant 2° XYZ CMFs) and three different illuminants: D65, A and F11. Thus, in total, we conducted six experiments. We interpolated the missing data in the Z component of the XYZ 2006 CMFs. We observed that the last 10nm in the data followed the exponential function which we used to interpolate Z.

First, we calculated the volume of a high precision OCS with the tolerance equal to 10^{-5} for the local error. This volume was calculated independently for the three illuminants and the two CMFs. The resulting six volumes provide benchmarks for the subsequent experiments i.e. they will be used to approximate the volume errors in our subsequent approximations of the object colour solids. The high precision OCS for the 2006 CMFs and the D65 illuminant can be seen in Figure 10.

Next, we proceed to the calculation of the OCSs' approximations using the three methods introduced in Section 1.

We approximated the OCS using the Schrodinger method as follows. We calculated the volume of the OCS using reflectances with zero, one and two transitions. We let the transitions be evenly distributed with distance $\Delta\lambda_1 = 4\text{nm}, \Delta\lambda_2 =$

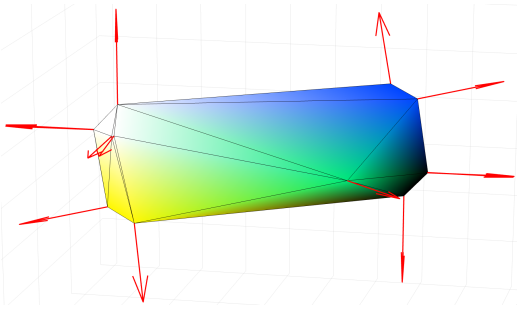

Figure 8: The regularised approximation of the OCS.

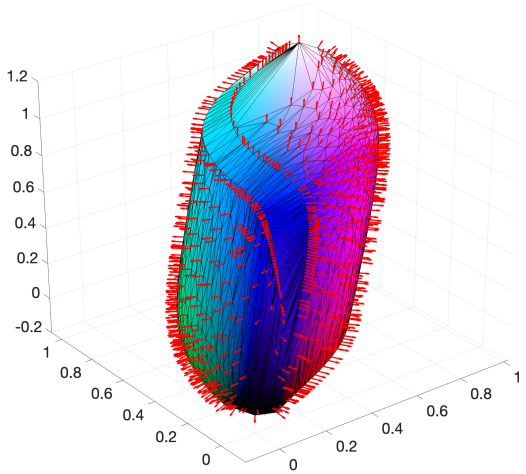

Figure 9: The regularised OCS is used to find a triangulation of the space ensuring the three vertices of each cell have similar colours. It also reveals that the two sheets comprising the OCS are smoothly connected in the white and black points and along the meridians. Calculated for the XYZ 2006 CMFs and the D65 illuminant.

6nm, $\cdots$, $\Delta\lambda_{14} = 30$nm within the limits of the visual spectrum from 390 to 730nm. We then calculated the volumes $V_{S,\Delta\lambda_i}$ for $i = 1, 2, \ldots, 14$.

For the OCS approximations utilising the Random Spherical Sampling method [5, 7], we used two times the number of samples as for the Schrodinger method. We used the version of the Random Spherical Sampling which utilises the set of orthonormal colour system spectra [7]. We then removed samples so that the corresponding OCS vertices are unique which resulted in the removal of approximately every second sample.

As to the new method presented in this paper, we also calculated fourteen volume approximations in each of the six experiments analogously to the two earlier methods. Here, we use the volume differences from the Schrodinger method as tolerances calculated using the formula $V_{S,\Delta\lambda_1} - V_{S,\Delta\lambda_i} + d$. We used the experimental value of $d = 1.7 \times 10^{-3}$ to avoid the difference to become zero.

Figure 11 shows the results of our experiments. The linearity of plots in Figure 11 suggest that the error of the benchmark high precision OCS is small. We see that the new method needs significantly fewer samples than both the Random Spherical Sampling method and the Schrodinger methods. The advantage of our method is greater for the F11 light source than for the other two illuminants. The choice of color matching functions does not seem to have a significant impact on the results.

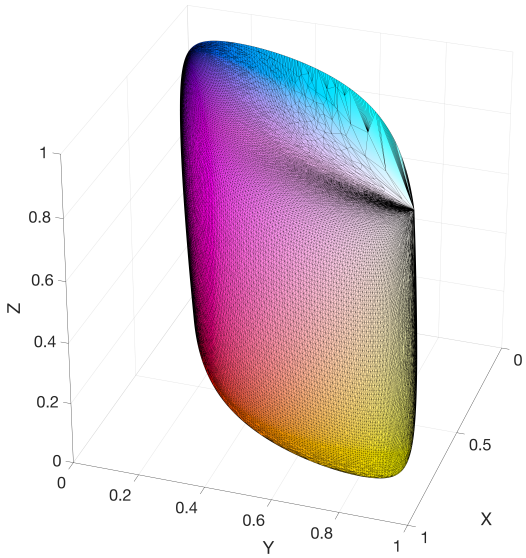

Figure 10: The high precision OCS approximation with 43864 unique vertices and 270,649 regular cells. The D65 illuminant and the 2006 CMF is applied. We used a error threshold of 10^{-5}.

In addition, we calculated the local error upper bounds for each cell in the OCS convex hull. Figure 14 shows the distribution of the error upper bounds.

Figure 12 shows the OCSs produced for the three methods being compared here for the CIE 1931 colour matching functions and the D65 illuminant. We can see that the two spherical sampling methods have more samples around high curvature areas than the Schrodinger method. Also, we can see that Optimised Spherical Sampling has more evenly sampled points around flat areas of the OCSs.

Figure 13 shows that our method only uses normal vectors in a limited region of the set of unit vectors. Note, that the shape and location of this region is independent of the illuminant. The Random Spherical Sampling method is less efficient in its choice of vector samples as many random samples lie outside the relevant area of the unit sphere.

5 Conclusions

We have demonstrated that our new method produces more accurate object colour solids with less samples than the two prior art methods. We admit that the generation of accurate object colour solids is not a significant problem as the prior art methods are faster and simpler than what we have proposed here. However, our method teaches us about the surface geometry of the OCSs as well as explicitly measures the underlying approximation errors. Acknowledging these advantages, the main reason for this ongoing work is our intention to use some of the observations regarding the error of the volume approximations for improving our understanding of the accuracy of approximations of the more relevant metamer mismatch volumes, which will be the subject of our future work.

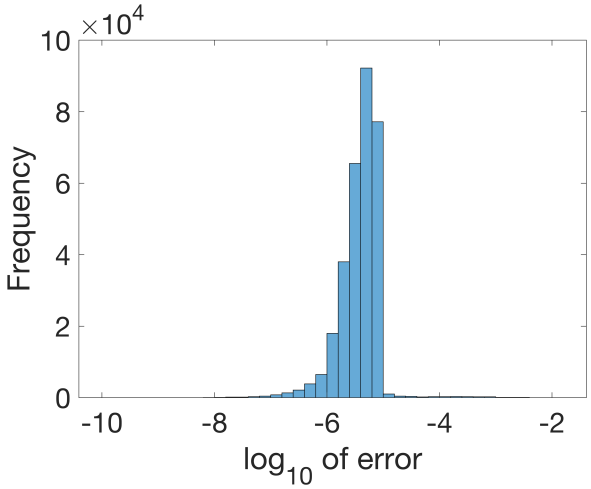

Figure 14: Histogram showing the upper bound error distribution for a high precision OCS approximation calculated for the CIE 1931 CMFs and the D65 illuminant. Note, the sharp edge around the tolerance, which was set to 10^{-5}.

References

[1] Michael H. Brill. Erwin Schrödinger's color theory: translated with modern commentary. *Color Research & Application*, 43(4):619–620, 2018.

[2] Scott A. Burns. The location of optimal object colors with more than two transitions. *Color Research & Application*, 46(6):1180–1193, 2021.

[3] J. Guild and Joseph Ernest Petavel. The colorimetric properties of the spectrum. *Philosophical Transactions of the Royal Society of London. Series A, Containing Papers of a Mathematical or Physical Character*, 230(681-693):149–187, 1931.

[4] Alexander D. Logvinenko. An object-color space. *Journal of Vision*, 9(11):5–5, 10 2009.

[5] Michal Mackiewicz, Hans J. Rivertz, and Graham D. Finlayson. Computing the object colour solid using spherical sampling. `https://ueaeprints.uea.ac.uk/id/eprint/62975/1/PICS_2016_abstract_finlayson_mackiewicz_rivertz.pdf`, 2016. Progress in Colour Studies - UCL, London, United Kingdom.

[6] Michal Mackiewicz, Hans J. Rivertz, and Graham D. Finlayson. Metamer mismatch volumes using spherical sampling. In *Color and Imaging Conference*, volume 2017, pages 88–92, United States, September 2017. Society for Imaging Science and Technology. Color and Imaging Conference ; Conference date: 11-09-2017 Through 15-09-2017.

[7] Michal Mackiewicz, Hans J. Rivertz, and Graham D. Finlayson. Spherical sampling methods for the calculation of metamer mismatch volumes. *J. Opt. Soc. Am. A*, 36(1):96–104, Jan 2019.

[8] Erwin Schrödinger. Theorie der pigmente von größter leuchtkraft. *Annalen der Physik*, 367(15):603–622, 1920.

[9] T Smith and J Guild. The c.i.e. colorimetric standards and their use. *Transactions of the Optical Society*, 33(3):73, jan 1931.

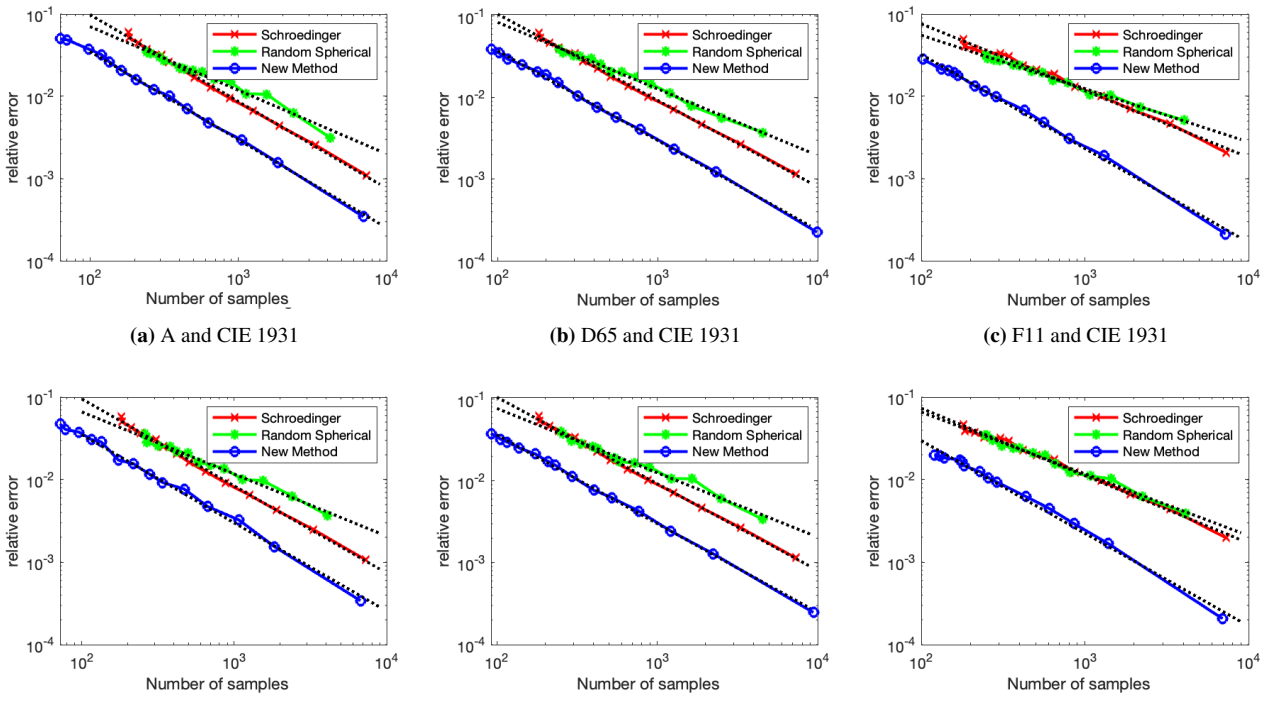

(a) A and CIE 1931 **(b)** D65 and CIE 1931 **(c)** F11 and CIE 1931

(d) A and CIE 2006 **(e)** D65 and CIE 2006 **(f)** F11 and CIE 2006

Figure 11: The relative errors for convex OCS approximations for the three different sampling methods. The first row of graphs shows the results from the CIE 1931 Colour matching functions. The second row shows the results we got by using the 2006 Colour matching functions.

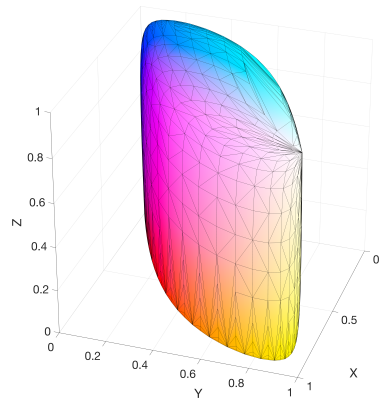

(a) Schrodinger method OCS. 1260 unique vertices

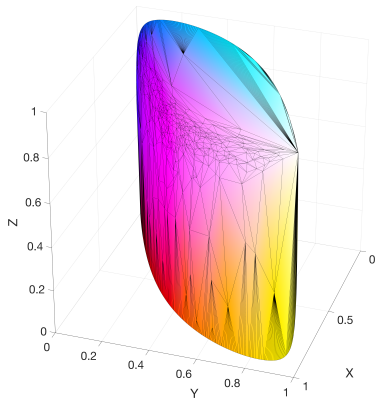

(b) Random spherical sampling. 1131 unique vertices.

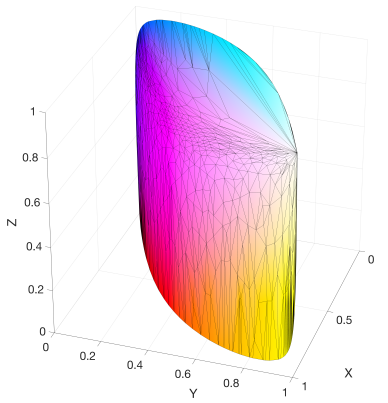

(c) Optimised spherical sampling. 1051 unique vertices.

Figure 12: The OCSs produced using (a) Schrodinger, (b) Random Spherical Sampling, (c) Optimised Spherical Sampling methods, for the CIE 1931 colour matching functions and the D65 illuminant. The XYZ-values have been normalised.

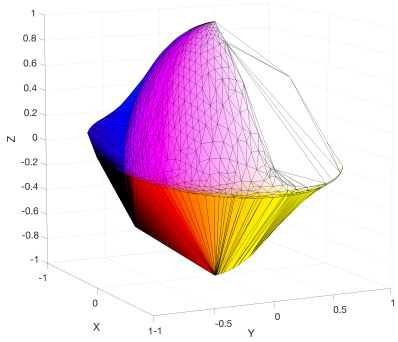

(a) A, proposed method. Regular triangulation. (CIE 1931)

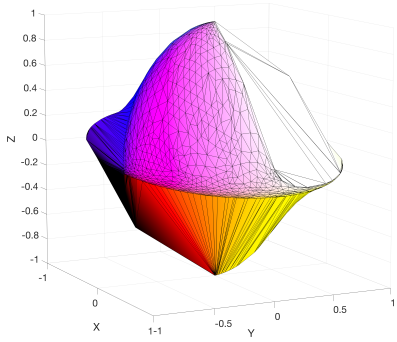

(b) D65, proposed method. Regular triangulation. (CIE 1931)

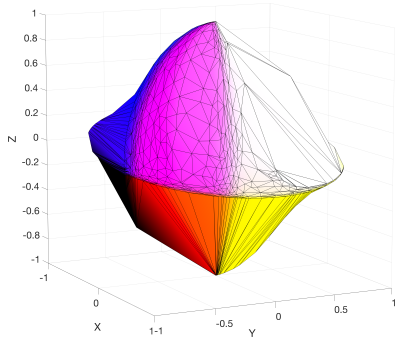

(c) F11, proposed method. Regular triangulation. (CIE 1931)

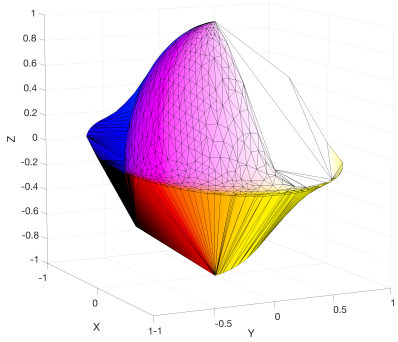

(d) A, proposed method. Regular triangulation. (CIE 2006)

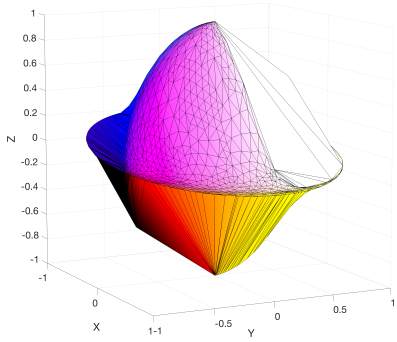

(e) D65, proposed method. Regular triangulation. (CIE 2006)

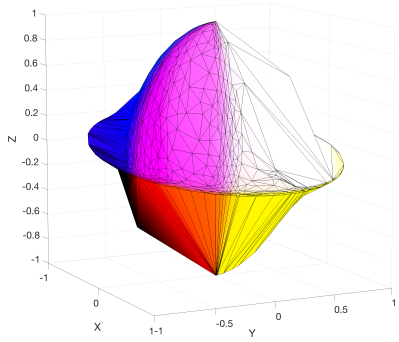

(f) F11, proposed method. Regular triangulation. (CIE 2006)

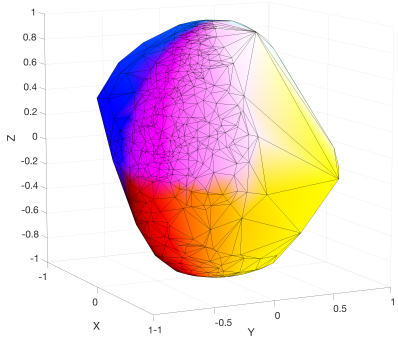

(g) A, random spherical sampling.

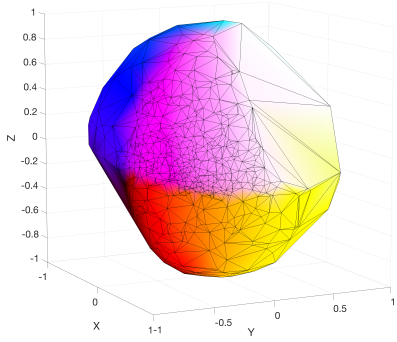

(h) D65, random spherical sampling.

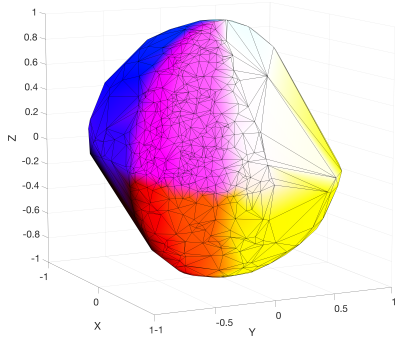

(i) F11, random spherical sampling.

Figure 13: These figures show the normal vectors as points on the unit sphere. The two upper rows show the normal vectors in the unit sphere produced by the new method. CIE 1931 CMFs are used in the upper row and CIE 2006 is used in the middle row. The lower row shows the vectors on the unit sphere produced by the Random Spherical Sampling method.